INTERNATIONAL JOURNAL FOR NUMERICAL METHODS IN FLUIDS, VOL. 6, 175–196 (1986)

# ROTATING DISK WITH UNIFORM SUCTION IN STREAMING FLOW

A. Z. SZERI, C. Y. LAI AND A. A. KAYHAN

*Department of Mechanical Engineering University of Pittsburgh. Pittsburgh, PA 15261, U.S.A.*

## SUMMARY

We investigate the flow as it occurs above a single rotating disk when uniform suction is applied at the disk surface. It has been demonstrated by others that at zero suction repeated branching of the solution occurs as the parameter $s$ is varied, where $s$ is the ratio of the angular velocity of the fluid at infinity to the angular velocity of the disk. We show multiplicity of solution also at $-0{\cdot}82 \leqslant \alpha \leqslant 1{\cdot}15$, where $\alpha$ is the suction parameter; for large absolute values of $\alpha$ the solution fails to turn back on itself and we obtain only the von Karman solution.

We then generalize the von Karman solution for flow above a single rotating disk with uniform suction to include non-axisymmetric solutions due to streaming at infinity. These solutions are continuous in an arbitrary parameter, the streaming velocity at infinity; for zero value of this parameter the asymmetric flow degenerates into the classical von Karman flow. Thus the classical solution is never isolated when considered within the framework of the Navier–Stokes equations: there are asymmetric solutions in every neighbourhood of the von Karman solution.

KEY WORDS Rotating Disk Asymmetric Flow Bifurcation Navier–Stokes Exact Solutions Multiplicity

## INTRODUCTION

It has been shown by von Karman[1] that two assumptions, namely that the flow is axisymmetric and that the axial velocity is invariant over planes parallel to a rotating disk, enable reduction of the Navier–Stokes equations to a set of ordinary differential equations which describe flow over the rotating disk. These equations remain valid also when there is uniform suction or blowing through the disk, on account of the axial velocity being independent of the radial co-ordinate. This was first pointed out by Batchelor,[2] and Stuart[3] gave the first solution to the problem. For small values of the suction parameter $\alpha$, where $\alpha\sqrt{(\nu\omega)}$ is the suction velocity and $\omega$ represents disk rotation, Stuart employed the Adams–Bashforth method used earlier by Cochran[4] for zero suction. For $\alpha > 1$ the solution was expanded in inverse powers of $\alpha$.

The von Karman equations remain applicable even when the fluid at infinity is rotating in a rigid body mode. Solutions have been obtained for various values of $s$ by Rogers and Lance[5] and others. However, it appeared to be not possible to find solutions in the parameter range $-0{\cdot}160 > s > -1{\cdot}4351$. At $s = -1{\cdot}4351$ the solution of the equations was found to become singular by Weidman and Redekopp[6], and Zandbergen and Dijkstra[7] showed that branching occurs at $s = -0{\cdot}16054$. Lentini and Keller[8] find that at least four families of solutions exist and conjecture existence of an infinite sequence of solutions. Suction, when it is applied, reduces the magnitude of both the radial and the azimuthal velocity components and promotes stability. Rogers and Lance[5] investigated the problem of the fluid rotating at infinity at equal rate but in the opposite sense from the disk and found physically acceptable solutions for $\alpha \geqslant 0{\cdot}6$.

0271–2091/86/040175–22$11.00

*Received February 1985*
*Revised 10 September 1985*

All of the above studies employed the classical assumptions of von Karman. Recently, however, Berker[9] considered the flow between corotating disks and established a one-parameter family of solutions. The only axisymmetric solution in this family is the rigid body motion, thus it is just this solution that would follow from von Karman's assumptions. Following Berker, Parter and Rajagopal[10] re-examined the classical problem of flow between rotating disks. They proved the existence of a one-parameter family of solutions for flow between two disks rotating about a common axis, or about distinct axes. These flows were calculated by Lai, Rajagopal and Szeri[11] for various values of $s$, where $s$ is now the ratio of disk rotational velocities. This work was extended by Lai, Rajagopal and Szeri[12] to flow in the semi-infinite interval above a single rotating disk.

In the present paper we study asymmetric flows above a rotating disk when uniform suction is applied at the disk. These asymmetric flows are obtained by superposition of the axisymmetric von Karman swirling flow in the presence of suction and a pseudo-plane motion, the velocity field of which has Cartesian components $\{g(z)\sqrt{(v\omega)}, -f(z)\sqrt{(v\omega)}, 0\}$. At infinity the velocity assumes the value of $\{0, -C\sqrt{(v\omega)}, 0\}$ where $C$ is an arbitrary constant. Hence, at $s = 0$ our generalized flow is obtainable by placing a rotating disk into a fluid that is streaming uniformly in the $y < 0$ direction with velocity $C\sqrt{(v\omega)}$. The functions $g(z)$ and $f(z)$ are defined by variable-coefficient linear ordinary differential equations, with coefficients depending on the von Karman solution $\{F(z), G(z), H(z)\}$ and on the constant $C$. Whenever there exist solutions to the von Karman problem we can, in the light of the work of Parter and Rajagopal,[10] proceed with determining the functions $\{f(z), g(z)\}$. These functions are continuous in $C$; thus symmetric solutions of the von Karman problem are never isolated when considered within the scope of the full Navier–Stokes equations; there are asymmetric solutions in every neighbourhood of the von Karman solutions.

The von Karman problem itself leads to a multiplicity of solutions. These solutions were already investigated at zero suction.[5–8] We demonstrate here repeated branching for non-zero suction; with $\alpha = 1$ first branching occurs at $s = -0{\cdot}257795$ and second branching takes place in the neighbourhood of $s = 0{\cdot}0750$. However, for $\alpha > 1{\cdot}154$ we were unable to find more than one solution to the von Karman flow. For this value of the suction parameter the solution fails to turn back on itself. For uniform blowing (negative suction) we demonstrate the first branch for $\alpha = -1$, $-2$, $-3$, $-4$ and the second branch for $\alpha = -0{\cdot}6$, $-0{\cdot}76$ and $-0{\cdot}82$.

## GOVERNING EQUATIONS

In this study of flow above a rotating disk we employ cylindrical polar co-ordinates $\{x^1, x^2, x^3\}$. The disk is located in $x^3 = 0$. We further define a non-dimensional co-ordinate system $\{r, \theta, z\}$ where

$$r = x^1\sqrt{(\omega/v)}; \theta = x^2; z = x^3\sqrt{(\omega/v)}. \tag{1}$$

The disk angular velocity is $\omega$, $v$ is the kinematic viscosity and the angular velocity of the fluid as $z \to \infty$ is $s\omega$.

In an attempt to extend the von Karman solutions to include flows with uniform streaming in the $y < 0$ direction at infinity, we superpose a pseudo-plane velocity field with Cartesian components $\{g(z)\sqrt{(v\omega)}, -f(z)(v\omega), 0\}$ on the von Karman swirling flow. The required condition at infinity will be satisfied if $g(z) \to 0$, $f(z) \to$ constant and $s \to 0$ as $z \to \infty$.

We thus seek solutions of the non-dimensional Navier–Stokes equations in the form

$$\bar{u}(r, \theta, z) = F(z) + \frac{1}{r}[g(z)\cos\theta - f(z)\sin\theta], \tag{2a}$$

$$\bar{v}(r, \theta, z) = G(z) - \frac{1}{r}[g(z)\sin\theta + f(z)\cos\theta], \tag{2b}$$

$$\bar{w}(z) = H(z). \tag{2c}$$

Here we put $\{u, v, w\} = x^1\omega\{\bar{u}, \bar{v}, (1/r)\bar{w}\}$ for the velocity field. The overscore bar signifies a non-dimensional quantity. The condition of incompressibility, div $\mathbf{v} = 0$, is identically satisfied by the velocity field $\mathbf{v} = \{u, v, w\}$ provided we allow for the relationship

$$F(z) = -\frac{1}{2}\frac{dH}{dz}. \tag{3}$$

The boundary conditions on the velocity are satisfied by specifying

$$\left.\begin{aligned} H = -\alpha, \quad \frac{dH}{dz} = 0, \quad G = 1 \\ f = g = 0 \end{aligned}\right\} \text{ at } z = 0, \tag{4a, 4b}$$

and

$$\left.\begin{aligned} \frac{dH}{dz} = 0, \quad G = s \\ f = C, \quad g = 0 \end{aligned}\right\} \text{ at } z \to \infty. \tag{5a, 5b}$$

However, these conditions are not sufficient to determine the solution uniquely. It is also necessary to assume that both $H'$ and $H''$ vanish as $z \to \infty$.[5]

We make use of the work of Lentini and Keller[8] here and require asymptotic conditions to be satisfied at some finite value of $z$, say $z_\infty$, in place of (5a). But to expedite calculations, first transform the semi-infinite interval $z \geqslant 0$ into the unit interval $0 \leqslant \bar{z} \leqslant 1$, where $\bar{z} = z/z_\infty$.

Substituting the velocity profile, written now in terms of the normalized co-ordinate $\bar{z}$, into the appropriate form of the non-dimensional Navier–Stokes equations we are led to the following system of ordinary differential equations:[1,2]

$$H''' - z_\infty HH'' + \tfrac{1}{2}z_\infty H'^2 - 2z_\infty^3(G^2 - s^2) = 0, \tag{6a}$$

$$G'' - z_\infty(G'H - GH') = 0, \tag{6b}$$

$$f''' - z_\infty Hf'' - \tfrac{1}{2}z_\infty(H'f' - H''f) + z_\infty^2(Gg)' = 0, \tag{7a}$$

$$g''' - z_\infty Hg'' - \tfrac{1}{2}z_\infty(H'g' - H''g) - z_\infty^2(Gf)' = 0. \tag{7b}$$

The first two of these equations (6) do not contain either $f(z)$ or $g(z)$; they represent the axisymmetric swirling flow of von Karman. The remaining two equations (7) are linear and are the conditions under which the pseudo-plane velocity field $\{g(z)\sqrt{(v\omega)}, -f(z)\sqrt{(v\omega)}, 0\}$ is compatible with the Navier–Stokes equations.

The boundary conditions which accompany equations (6) and (7) are obtained from (4) and (5b) by transformation to $\bar{z}$:

at $\bar{z} = 0$:

$$H = -\alpha, \quad H' = 0, \quad G = 1, \tag{8a}$$

$$f = g = 0; \tag{8b}$$

At $\bar{z} = 1$:

$$f = C, \quad g = 0. \tag{8c}$$

In place of employing conditions (5a) at $\bar{z} = 1$, we specify there the asymptotic conditions of Lentini and Keller:[8]

$$\frac{1}{z_\infty}[H_\infty + a(H_\infty, s)]H'(1) + \frac{1}{z_\infty^2}H''(1) - \frac{s}{a(H_\infty, s)}[G_\infty - s] = 0, \tag{9a}$$

$$\frac{b^2(H_\infty, s)}{z_\infty s}a(H_\infty, s)H'(1) + [H_\infty + a(H_\infty, s)](G_\infty - s) + \frac{1}{z_\infty}G'(1) = 0. \tag{9b}$$

Here $H_\infty = H(1)$, $G_\infty = G(1)$, and

$$\begin{aligned} a(H_\infty, s) &= \frac{1}{\sqrt{2}}[(H_\infty^4 + 4s^2)^{1/2} + H_\infty^2]^{1/2}, \\ b(H_\infty, s) &= \frac{1}{\sqrt{2}}[(H_\infty^4 + 4s^2)^{1/2} - H_\infty^2]^{1/2}. \end{aligned} \tag{10}$$

These conditions guarantee bounded solutions of the non-linear problem on the semi-infinite interval $z \geqslant 0$.

We need one more condition each on $f(z)$ and $g(z)$. The requirement for absence of a shear layer at infinity leads to

$$f' = g' = 0 \quad \text{as} \quad z \to \infty. \tag{11}$$

Clearly, other choices are possible.

It follows from the transformation $z \to \bar{z}$ that $(\mathrm{d}f/\mathrm{d}z) = (\mathrm{d}f/\mathrm{d}\bar{z})/z_\infty$; thus if $z_\infty \to \infty$ and $\mathrm{d}f/\mathrm{d}\bar{z} < k$ for some finite $k$, $\mathrm{d}f/\mathrm{d}z \to 0$ at any $z$. Therefore, the transformation $\bar{z} = z/z_\infty$ is acceptable only if there is rapid convergence of the solution as $z_\infty$ is increased from unity. That this is the case was demonstrated elsewhere.[12]

## NUMERICAL METHOD

We seek solutions to equations (6), (7), (8), (9) and (11) in the weak form

$$\{G, H, f, g\} = \sum_{j=1}^{N} \{G_j, H_j, f_j, g_j\}B_j(\bar{z}), \tag{12}$$

where $\{B_j(\bar{z})\}_{j=1}^N$ is a set of cubic B-splines defined on the partition

$$\pi: 0 = \bar{z}_1 < \bar{z}_2 < \cdots < \bar{z}_l < \bar{z}_{l+1} = 1, \tag{13}$$

with a knot sequence $\{t_k\}_{k=1}^{N+4}$ given by

$$\begin{aligned} \bar{z}_1 &= t_1 = t_2 = t_3 = t_4, \\ \bar{z}_2 &= t_5, \\ &\vdots \\ \bar{z}_l &= t_N, \\ \bar{z}_{l+1} &= t_{N+1} = t_{N+2} = t_{N+3} = t_{N+4}. \end{aligned} \tag{14}$$

Here $N$ is the dimension of the approximating subspace, calculated from

$$N = 4 + \sum_{i=2}^{l} (4 - v_i)$$

and $v_i = 3$, $2 \leqslant i \leqslant l$, is the smoothness index at the internal breakpoints.[13]

Satisfaction of the boundary conditions (8), (9a) and (11) yields

$$H_1 = -H_2 = -\alpha, \quad G_1 = 1, \quad f_1 = g_1 = 0, \tag{15a}$$

$$f_N = -f_{N-1} = C, \quad g_N = g_{N-1} = 0, \tag{15b}$$

and the asymptotic conditions (9a, b) take the form

$$\frac{1}{z_\infty}[H_N + a(H_N, s)]\left[(H_N - H_{N-1})B'_N\Big|_{\bar{z}_{l+1}} + \frac{1}{z_\infty^2}H_{N-2}B''_N\Big|_{\bar{z}_{l-1}} + H_{N-1}B''_N|_{\bar{z}_l} + H_N B''_N|_{\bar{z}_{l+1}}\right] - \frac{s}{a(H_N, s)}(G_N - s) = 0 \tag{15c}$$

and

$$\frac{1}{z_\infty}\frac{b^2(H_N, s)}{s}a(H_N, s)(H_N - H_{N-1})B'_N\Big|_{\bar{z}_{l+1}} + [H_N + a(H_N, s)](G_N - s) + \frac{1}{z_\infty}(G_N - G_{N-1})B'_N\Big|_{\bar{z}_{l+1}} = 0. \tag{15d}$$

Here

$$a(H_N, s) = \frac{1}{\sqrt{2}}[(H_N^4 + 4s^2)^{1/2} + H_N^2]^{1/2},$$

$$b(H_N, s) = \frac{1}{\sqrt{2}}[H_N^4 + 4s^2)^{1/2} - H_N^2]^{1/2}. \tag{16}$$

Substituting (12) into equations (6) and (7), multiplying through by the test sets

$$\begin{aligned} \tau^H &= \{B_k(\bar{z}): \quad 3 \leqslant i \leqslant N-1\}, \\ \tau^G &= \{B_l(\bar{z}): \quad 2 \leqslant j \leqslant N-1\}, \\ \tau^f &= \{B_m(\bar{z}): \quad 2 \leqslant k \leqslant N-2\}, \\ \tau^g &= \{B_n(\bar{z}): \quad 2 \leqslant l \leqslant N-2\}, \end{aligned} \tag{17}$$

and integrating from $\bar{z} = 0$ to $\bar{z} = 1$ yields the following four sets of algebraic equations:

$$\sum_{i=1}^{N}\{z_\infty^{-3}H_i\underline{\bar{z}}_{ki}^{(4)} - 2s^2\underline{\bar{z}}_{ki}^{(0)}\} + \sum_{i,j=1}^{N}\{z_\infty^{-2}H_iH_j[\underline{\bar{Z}}_{kij}^{(2)} - \tfrac{1}{2}\underline{\bar{Z}}_{kij}^{(3)}] + 2G_iG_j\underline{\bar{Z}}_{kij}^{(0)}\} = 0, \tag{18a}$$

$$\sum_{i=1}^{N}G_i\underline{\bar{z}}_{li}^{(2)} + z_\infty\sum_{i,j=1}^{N}G_iH_j[\underline{\bar{Z}}_{lij}^{(1)} - \underline{\bar{Z}}_{lji}^{(1)}] = 0, \tag{18b}$$

$$\sum_{j=1}^{N}f_j\left\{z_\infty\sum_{i=1}^{N}H_i[\tfrac{1}{2}\underline{\bar{Z}}_{mji}^{(2)} - \tfrac{1}{2}\underline{\bar{Z}}_{mij}^{(3)} - \underline{\bar{Z}}_{mij}^{(2)}] - \underline{\bar{z}}_{mj}^{(4)}\right\} + z_\infty^2\sum_{i,j=1}^{N}G_ig_j[\underline{\bar{Z}}_{mij}^{(1)} + \underline{\bar{Z}}_{mji}^{(1)}] = 0, \tag{18c}$$

$$\sum_{j=1}^{N}g_j\left\{z_\infty\sum_{i=1}^{N}H_i[\tfrac{1}{2}\underline{\bar{Z}}_{nji}^{(2)} - \tfrac{1}{2}\underline{\bar{Z}}_{nij}^{(3)} - \underline{\bar{Z}}_{nij}^{(2)}] - \underline{\bar{z}}_{nj}^{(4)}\right\} - z_\infty^2\sum_{i,j=1}^{N}f_jG_i\{\underline{\bar{Z}}_{nij}^{(1)} + \underline{\bar{Z}}_{nji}^{(1)}] = 0, \tag{18d}$$

$$3 \leqslant k \leqslant N-1, \quad 2 \leqslant l \leqslant N-1, \quad 2 \leqslant m \leqslant N-2, \quad 2 \leqslant n \leqslant N-2.$$

The spline inner products $\underline{\bar{z}}_{jk}^{(0)}, \ldots, \underline{\bar{Z}}_{ijk}^{(3)}$ have the definitions

$$\begin{aligned} \underline{\bar{z}}_{jk}^{(p)} &= \int_0^1 B_j^{(b)}(\bar{z})B_k^{(c)}(\bar{z})\mathrm{d}\bar{z}, \\ \underline{\bar{Z}}_{ijk}^{(p)} &= \int_0^1 B_i^{(a)}(\bar{z})B_j^{(b)}(\bar{z})B_k^{(c)}(\bar{z})\mathrm{d}\bar{z}, \end{aligned} \tag{19}$$

$$a \leqslant b \leqslant c,$$
$$p = a + b + c + 1 \quad (\text{if } b \neq 0) + 2(\text{if } a \neq 0).$$

The first solution of the non-linear system (15), (18) is calculated on a uniform partition. This solution is then improved by employing the adaptive mesh selection strategy of de Boor.[13,14] The idea behind this strategy is to concentrate the breakpoints in locations of expected large variations in the solution $H(\bar{z})$. To this end the solution $H(\bar{z})$ obtained on a uniform partition is represented by the cubic spline interpolant

$$P_n(\bar{z}) = \sum_{k=1}^{4} \frac{C_{k,n}}{n!}(\bar{z} - \tau_n)^{k-1}. \tag{20}$$

To evaluate the $C_{k,n}$ we employ a subroutine by de Boor.[13] Calculation of $H(\bar{z})$ is based on the $C_{k,n}$ and we choose

$$h(\bar{z}) = \begin{cases} \dfrac{2|\Delta H_{3/2}|}{(\bar{z}_3 - \bar{z}_1)}, & \text{on } [\bar{z}_1, \bar{z}_2], \\ \dfrac{\Delta H_{i-1/2}}{(\bar{z}_{i+1} - \bar{z}_{i-1})} + \dfrac{\Delta H_{i+1/2}}{(\bar{z}_{i+2} - \bar{z}_i)}, & \text{on } [\bar{z}_i, \bar{z}_{i+1}],\ 2 \leqslant i \leqslant N-1, \\ \dfrac{2|\Delta H_{l-1/2}|}{(\bar{z}_{l+1} - \bar{z}_{l-1})}, & \text{on } [\bar{z}_l, \bar{z}_{l+1}]. \end{cases} \tag{21}$$

Here

$$H_{i+1/2} = H(z)^{(k-1)}, \quad \text{on } [\bar{z}_i, \bar{z}_{i+1}], \tag{22}$$
$$\Delta H_{i-1/2} = H_{i+1/2} - H_{i-1/2}.$$

The new partition is defined then with the aid of a piecewise linear function $\kappa$, where

$$\kappa(\bar{z}) = \int_0^{\bar{z}} [h(s)]^{1/k} ds; \quad \kappa(1) = \int_0^1 [h(s)]^{1/k} ds. \tag{23}$$

The iteration $n = 1, 2, 3, \ldots$ is described by

$$\bar{z}_i^{(n)} = \frac{1}{\kappa(\bar{z})}\left[(i-1)\frac{\kappa(1)}{l^{(n)}}\right]; \quad 1 \leqslant i \leqslant l^{(n)} + 1, \tag{24}$$

where $l^{(n)}$ is the number of the new subintervals.

## RESULTS AND DISCUSSION

The accuracy of the Galerkin method with B-spline test functions has been discussed elsewhere.[11,12] In particular, in Reference 12 we investigated the effect of (i) the number of splines $N$ in the expansion (12), (ii) the grading of the mesh and (iii) the positioning of the far boundary $z_\infty$. Here we only detail the use of the adaptive mesh generation scheme.

The first solution, when employing adaptive mesh grading, is obtained on a uniform partition. For $s = 0$ and $\alpha = 2$, solution for branch I on a uniform partition with $N = 63$ and $z_\infty = 15$ yields $F_{\max} = 0{\cdot}0280296$ for maximum dimensionless radial velocity, as shown in the first row of Table I. Results for $n = 1$ in equation (24) are displayed in the row with iteration no. 1 of the same table. Here $|\varepsilon|$ is the norm of the residue of the non-linear equations. The residues $R_1$ and $R_2$, on the other

Table I. Iteration on breakpoint distribution (branch I, $s = 0$, $\alpha = 2$, $z_\infty = 15$, $N = 63$)

| | | | | |
|---|---|---|---|---|
| Uniform mesh | $0{\cdot}280296 \times 10^{-1}$ | $0{\cdot}127481 \times 10^{-11}$ | $0{\cdot}678754 \times 10^{-2}$ | $0{\cdot}731081 \times 10^{-1}$ |
| 1 | $0{\cdot}296251 \times 10^{-1}$ | $0{\cdot}259244 \times 10^{-9}$ | $0{\cdot}667045 \times 10^{-1}$ | $0{\cdot}105790 \times 10^{-2}$ |
| 2 | $0{\cdot}296042 \times 10^{-1}$ | $0{\cdot}370950 \times 10^{-9}$ | $0{\cdot}616390 \times 10^{-1}$ | $0{\cdot}688415 \times 10^{-3}$ |
| 3 | $0{\cdot}296099 \times 10^{-1}$ | $0{\cdot}420485 \times 10^{-9}$ | $0{\cdot}140154 \times 10^{-1}$ | $0{\cdot}132959 \times 10^{-2}$ |
| 4 | $0{\cdot}296056 \times 10^{-1}$ | $0{\cdot}457967 \times 10^{-10}$ | $0{\cdot}467392 \times 10^{-1}$ | $0{\cdot}189926 \times 10^{-2}$ |
| 5 | $0{\cdot}296171 \times 10^{-1}$ | $0{\cdot}203562 \times 10^{-9}$ | $0{\cdot}576451 \times 10^{-1}$ | $0{\cdot}204999 \times 10^{-2}$ |
| Stuart[3] | 0·0295 | — | — | — |

hand, have the following definitions:[7]

$$R_1 = \left| H''^2(0) - G'^2(0) - 4\int_0^\infty H(H''^2 - G'^2)\mathrm{d}z \right|,$$
$$R_2 = \left| H''(0)G'(0) + \tfrac{2}{3}s^3 - s^2 + \tfrac{1}{3} - 4\int_0^\infty HH''G'\mathrm{d}z \right|. \tag{25}$$

They are obtained from equation (6) by simple manipulations. Table I also contains a result from Stuart's work.[3]

The effect of the suction parameter on the von Karman flow for the branch I solution is shown in Figures 1–3. These solutions have already been given by Stuart.[3] The corresponding solutions for branch II are displayed in Figures 4–6. The main feature of the branch II solutions in comparison with branch I solutions is the creation of two cells. Cells are regions bounded by $z =$ constant planes on which the axial velocity vanishes. The branch II solution of $\alpha = 0$ was obtained from the branch I solution of $\alpha = 0$ by continuation in $s$, starting from $s = 0$. Having obtained the branch II

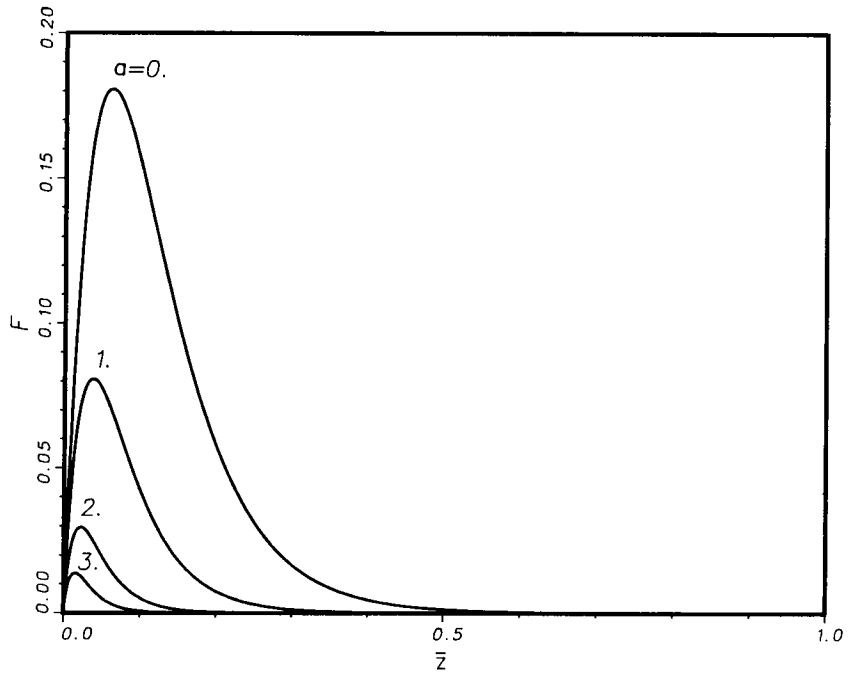


Figure 1. Dimensionless radial velocity of symmetric flow. Branch I at $s = 0$

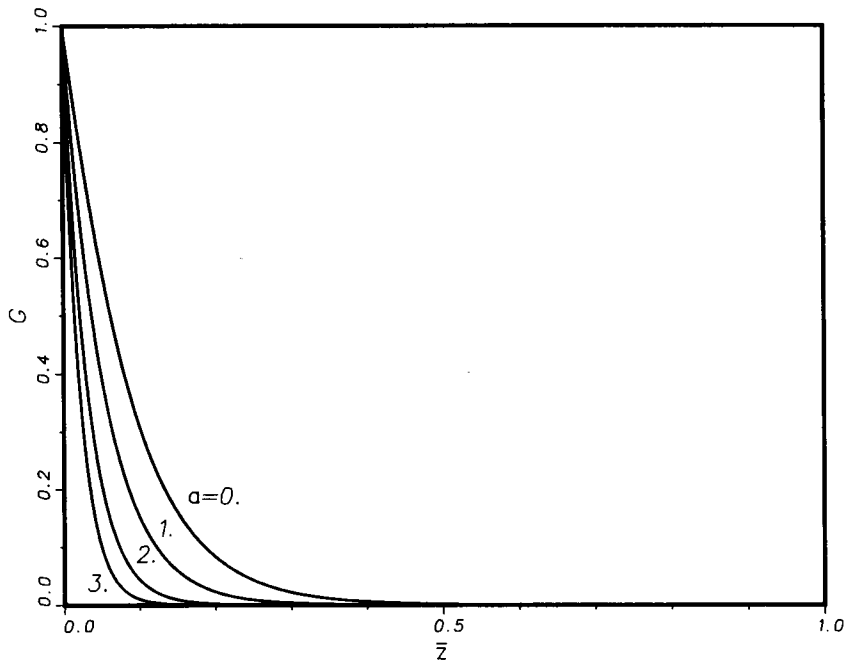


Figure 2. Dimensionless azimuthal velocity of symmetric flow. Branch I at $s = 0$

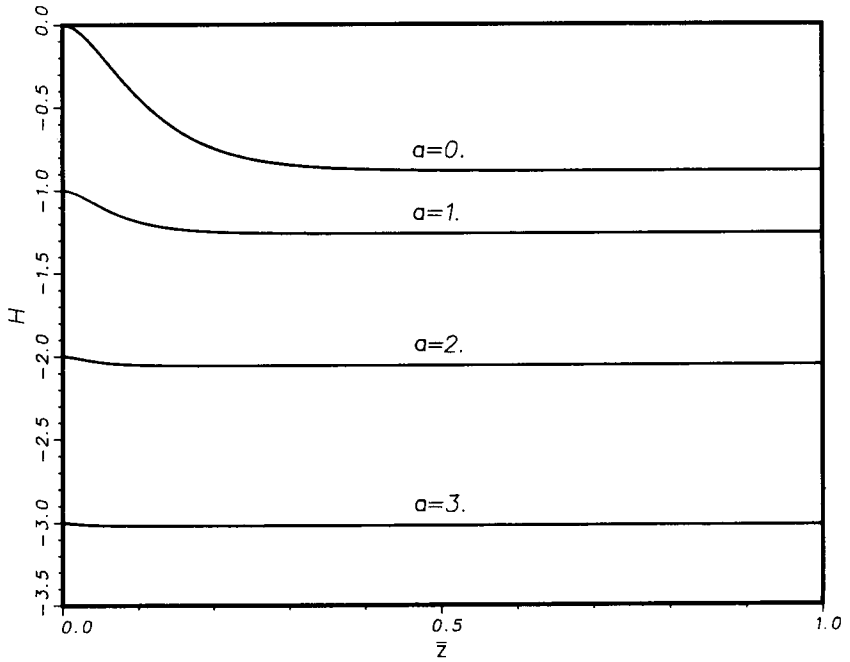


Figure 3. Dimensionless axial velocity of symmetric flow. Branch I at $s = 0$

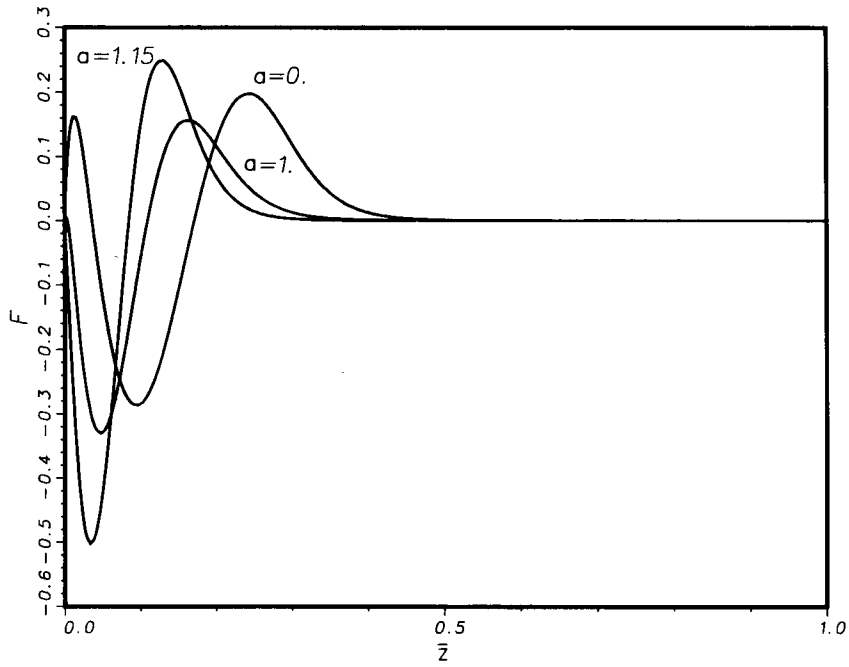


Figure 4. Dimensionless radial velocity of symmetric flow. Branch II at $s = 0$

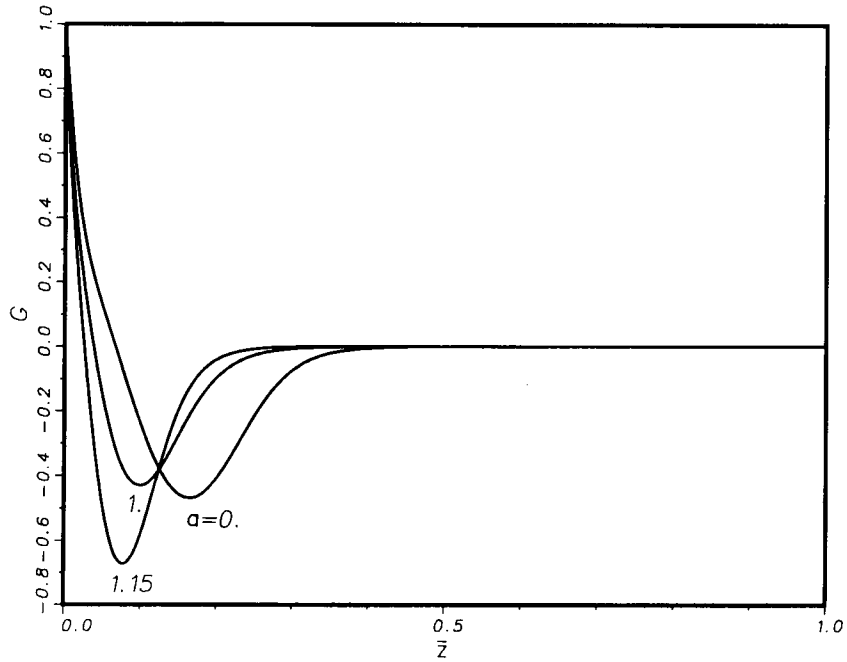


Figure 5. Dimensionless aximuthal velocity of symmetrric flow. Branch II at $s = 0$

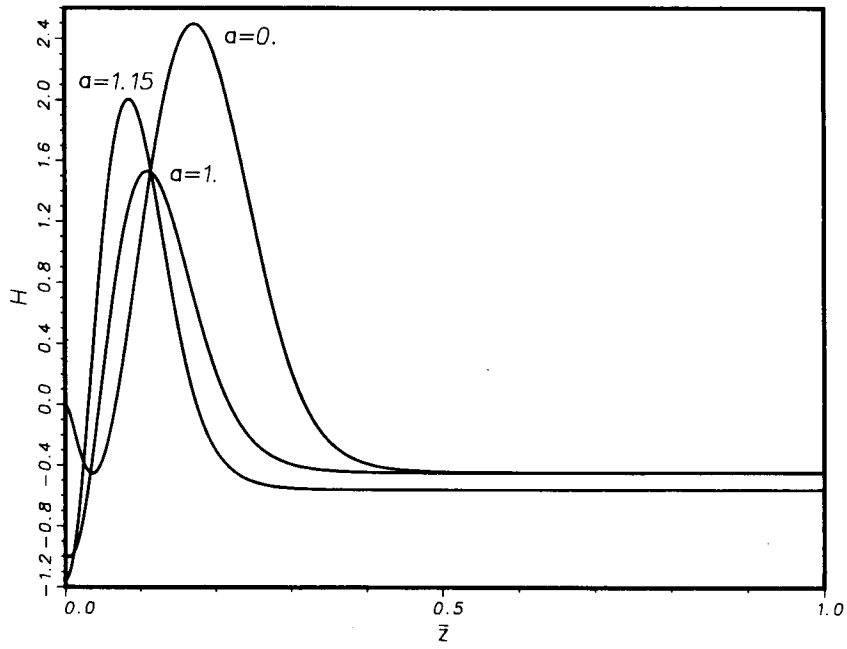


Figure 6. Dimensionless axial velocity of symmetric flow. Branch II at $s = 0$

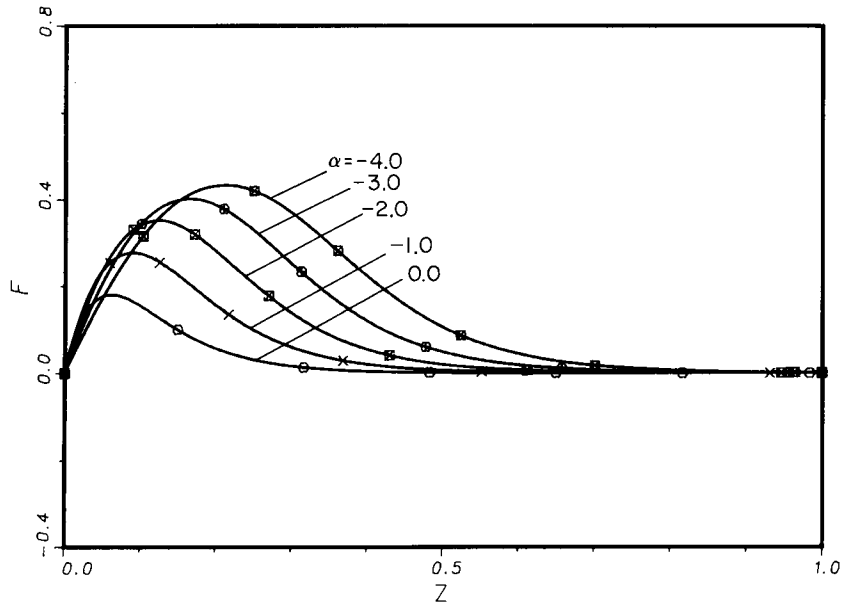


Figure 7. Dimensionless radial velocity of symmetric flow. Branch I at $s = 0$

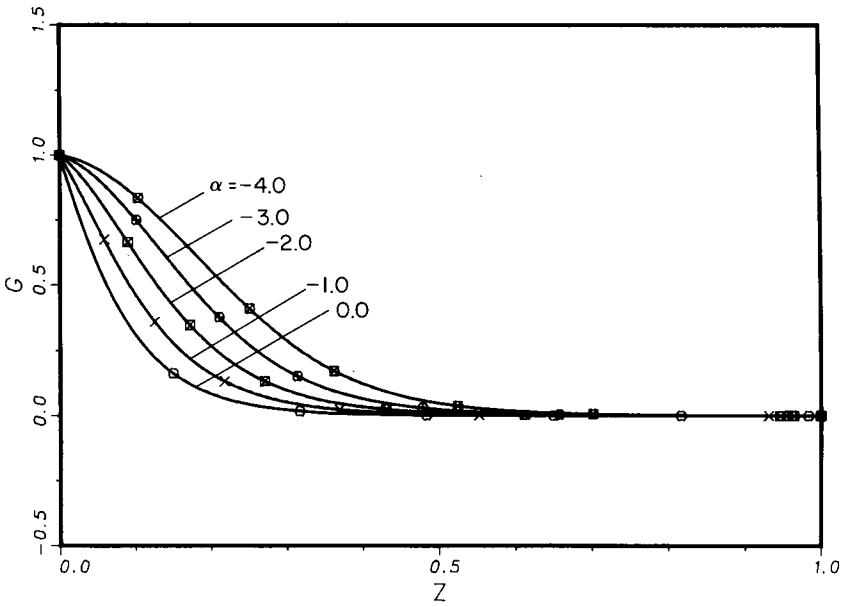


Figure 8. Dimensionless aximuthal velocity of symmetric flow. Branch I at $s = 0$

solution for $\alpha = 0$ and $s = 0$, other branch II solutions for $s = 0, \alpha > 0$ were reached via continuation in $\alpha$. By continuation, say in $s$, we mean the process whereby the initial values in the Newton iteration for the solution of the non-linear equations (18) at $s + \Delta s$ are supplied by the solution of (18) that was obtained at $s$. When continuing the solution in $s$ and upon reaching a branch point, as manifested by $ds/dH_\infty = 0$, we redefine the non-linear algebraic system (18) by regarding $s$ as the unknown. The solution is then continued in $H_\infty$ for a short distance.

Figures 4–6 contain branch II solutions at the parameter values $s = 0$ and $\alpha = 0, 1, 1{\cdot}15$. We were unable to obtain convergence for Newton's method of (18) for $\alpha > 1{\cdot}154$. Note that these solutions show surprisingly strong boundary layer structure as $\alpha$ increases.

Figures 7–12 display non-dimensional velocity profiles for negative suction, i.e. blowing. Branch I solutions are shown in the first three of these Figures; these Figures show a thickening of the boundary layer with increasing blowing velocity. For small to moderate blowing the second branch also exists, at least at zero fluid rotation at infinity. We were unable to obtain the second branch for $\alpha < -0{\cdot}82$. For $-0{\cdot}82 \leqslant \alpha \leqslant 0$ the velocity profiles are displayed in Figures 10–12.

Figure 13 displays the solution of equations (18 a, b) on the $\{s, \frac{1}{2}H_\infty\}$ plane. The curve marked $\alpha = 0$, i.e. flow with zero suction, was already obtained by Lentini and Keller.[8] This solution, proceeding to the left from the point $(0, -0{\cdot}4422)$ turns back on itself, with first branching occurring at $s = -0{\cdot}16054$. The solution curve cuts the $s = 0$ axis at $\frac{1}{2}H_\infty = -0{\cdot}630275$ when $\alpha = 1$, and first branching occurs at $s = -0{\cdot}257795$. For $s > -0{\cdot}16$ the solutions for $\alpha = 0$ and $\alpha = 1$ approach one another, as shown in Figure 13. becoming almost identical for positive rotation at infinity, $s > 0$. Second branching of the solution occurs at $s = 0{\cdot}07452$ when $\alpha = 0$ and at $s = 0{\cdot}075$ when $\alpha = 1$.

Starting from the point where the second branch of the $\alpha = 1$ curve intersects the $s = 0$ axis, we continued the solution in $\alpha$ to $\alpha > 1$ in order to locate the second branch of the solution for higher values of the suction velocity. The furthest we were able to proceed with this scheme was $\alpha = 1{\cdot}154$; our algorithm would not converge for values of $\alpha$ exceeding $1{\cdot}154$. We first reasoned that there

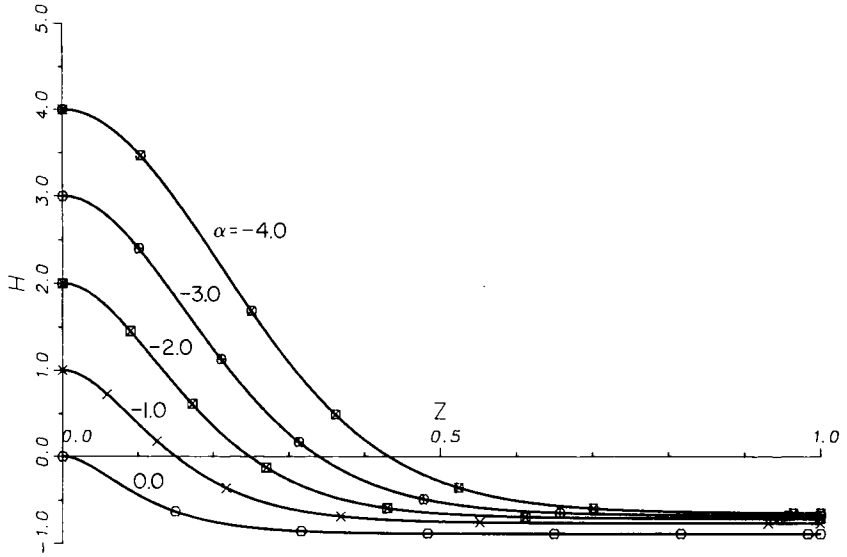


Figure 9. Dimensionless axial velocity of symmetric flow. Branch I at $s = 0$

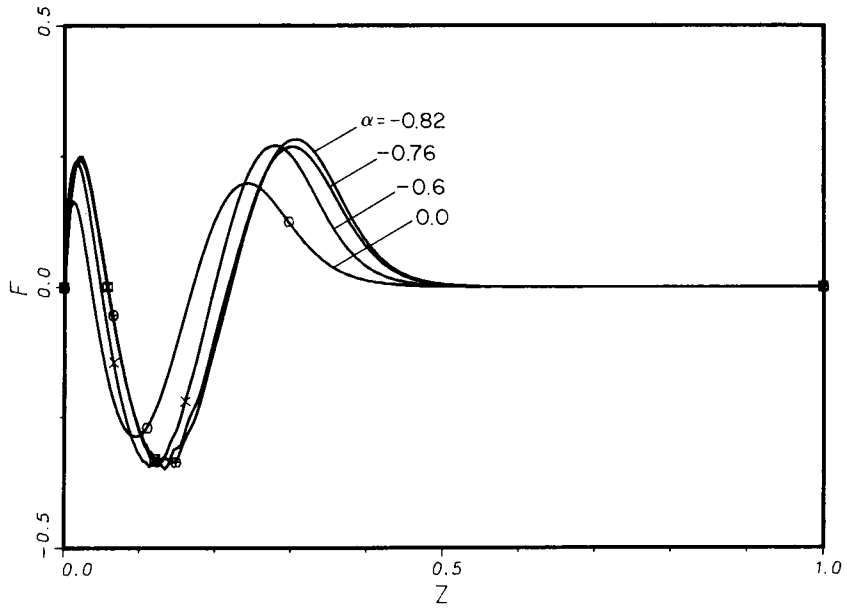


Figure 10. Dimensionless radial velocity of symmetric flow. Branch II at $s = 0$

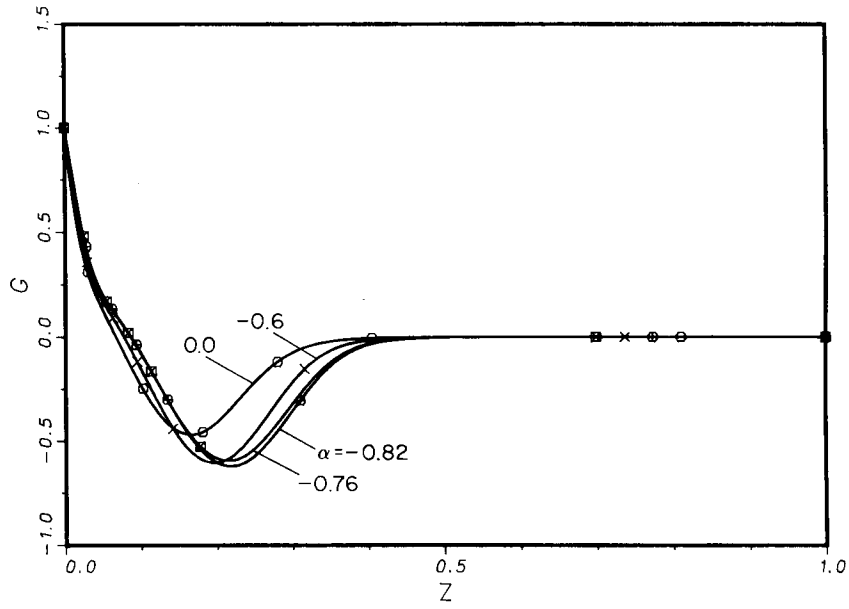


Figure 11. Dimensionless aximuthal velocity of symmetric flow. Branch II at $s = 0$

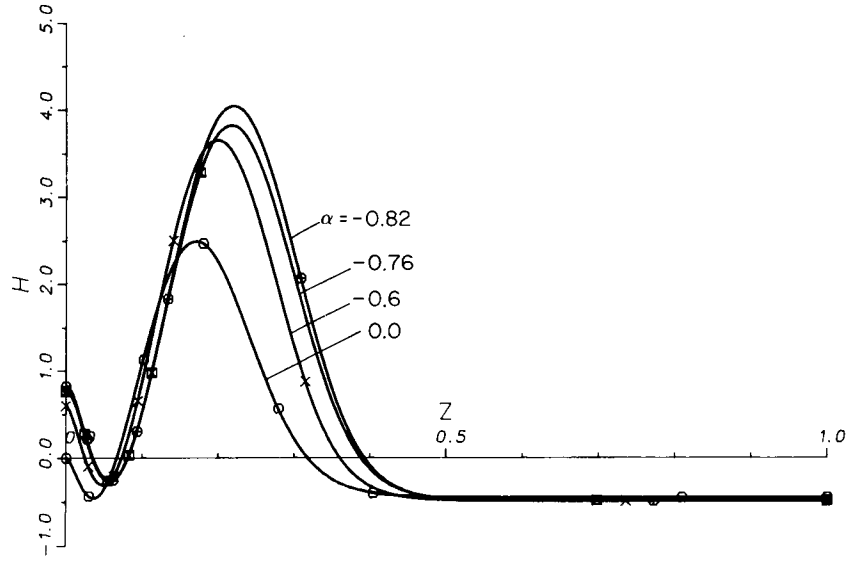


Figure 12. Dimensionless axial velocity of symmetric flow. Branch II at $s = 0$

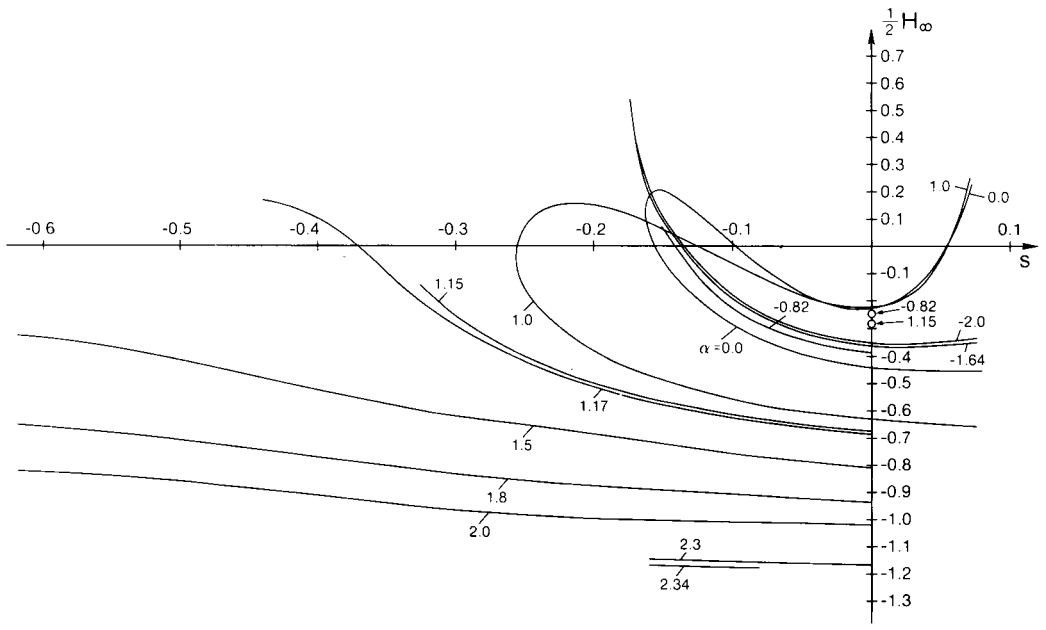


Figure 13. Axial flow at infinity: $-\frac{1}{2}H_\infty$ as a function of $s = \omega_\infty/\omega$

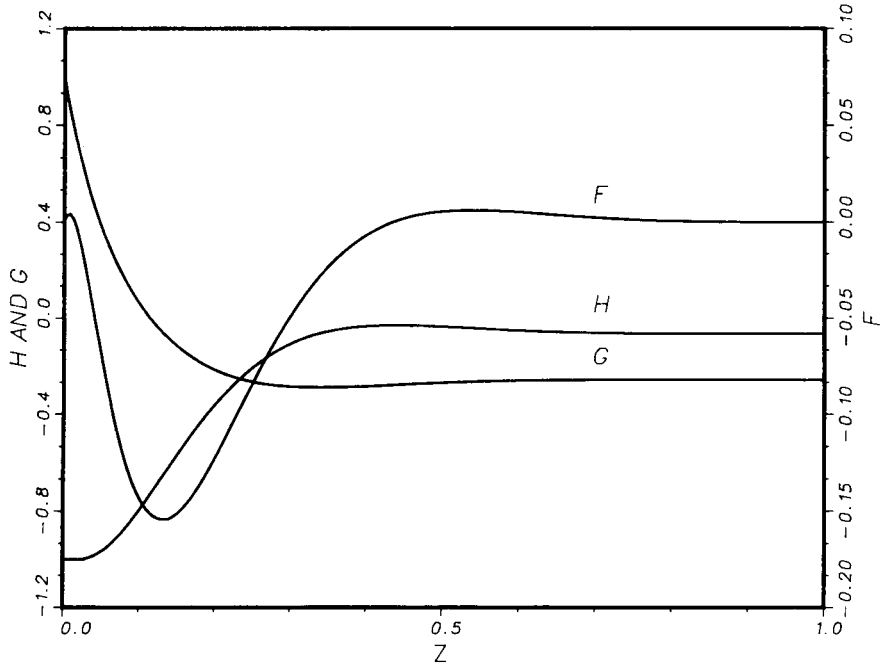


Figure 14. Symmetric flow with suction, $\alpha = 1$, at the first branching point, $s = -0{\cdot}257795$

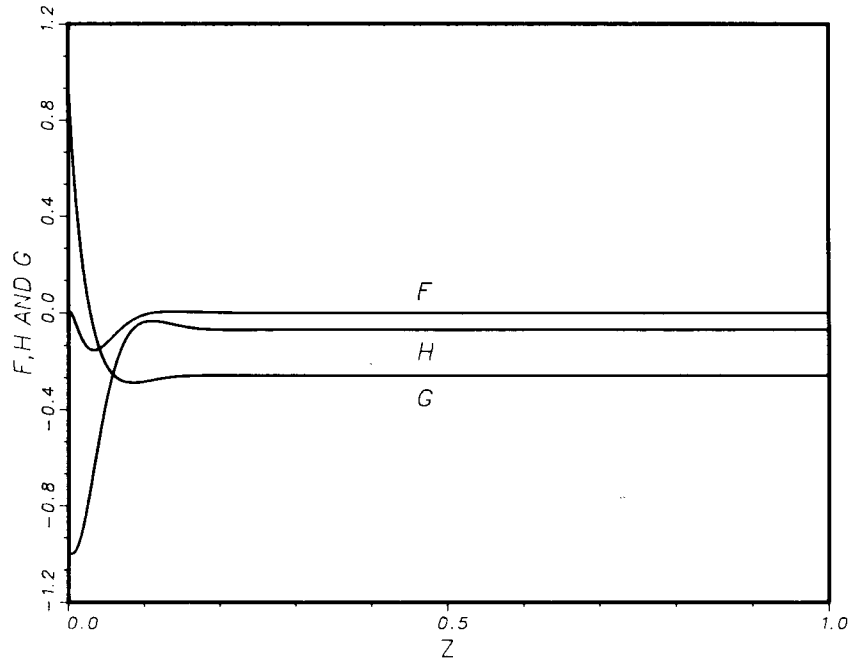


Figure 15. Symmetric flow with suction, $\alpha = 1$, at the second branching point, $s = 0{\cdot}0750$

existed a point of singularity in the neighbourhood of $\alpha = 1{\cdot}154$. Eventually, we performed calculations with $\alpha = 1{\cdot}5$, $1{\cdot}8$ and $2{\cdot}0$ on the first branch, obtaining the $s = 0$ point in each case by continuation in $\alpha$ from branch I along the $s = 0$ axis. The results of this effort are shown in Figure 13. With $a \geqslant 1{\cdot}5$ the solutions curves do not double back in our computations but become, instead, asymptotic to the $s < 0$ axis. Such behaviour of the solutions would explain the difficulty experienced earlier, when trying to locate the second branch of solution with $\alpha$ large.

First branching occurs at $s = -0{\cdot}257795$ when $\alpha = 1$. Figure 14 displays the von Karman solution at this value of $s$; here branches I and II coincide. To follow the evolution of the solution along the branch line we compare the branch I, $\alpha = 1$ curves of Figures 1–3, obtained at $s = 0$, with the curves in Figure 14, valid for $s = 0{\cdot}257795$ with branches I and II coinciding, with the branch II

Table II. Asymmetric flow, branch I: uniform streaming at infinity, $s = 0$ and uniform suction, $\alpha = 1$

| $\bar{z}$ | $F$ | $G$ | $-\frac{1}{2}H$ | $f$ | $g$ |
|---|---|---|---|---|---|
| 0·0 | 0·0 | 1·0 | 0·5 | 0·0 | 0·0 |
| 0·103026 | $0{\cdot}408676 \times 10^{-1}$ | 0·147543 | 0·594900 | 0·134454 | $-0{\cdot}306874 \times 10^{-1}$ |
| 0·206746 | $0{\cdot}665270 \times 10^{-2}$ | $0{\cdot}207746 \times 10^{-1}$ | 0·624935 | 0·266920 | $-0{\cdot}369101 \times 10^{-1}$ |
| 0·304315 | $0{\cdot}107114 \times 10^{-2}$ | $0{\cdot}328343 \times 10^{-2}$ | 0·629425 | 0·388877 | $-0{\cdot}338102 \times 10^{-1}$ |
| 0·398223 | $0{\cdot}181897 \times 10^{-3}$ | $0{\cdot}556140 \times 10^{-3}$ | 0·630130 | 0·501590 | $-0{\cdot}288417 \times 10^{-1}$ |
| 0·483917 | $0{\cdot}359297 \times 10^{-4}$ | $0{\cdot}110025 \times 10^{-3}$ | 0·630245 | 0·595378 | $-0{\cdot}239350 \times 10^{-1}$ |
| 0·627978 | $0{\cdot}231266 \times 10^{-5}$ | $0{\cdot}721715 \times 10^{-5}$ | 0·630270 | 0·697062 | $-0{\cdot}156302 \times 10^{-1}$ |
| 0·707126 | $0{\cdot}482798 \times 10^{-6}$ | $0{\cdot}161002 \times 10^{-5}$ | 0·630275 | 0·672267 | $-0{\cdot}111890 \times 10^{-1}$ |
| 0·828308 | $0{\cdot}178814 \times 10^{-7}$ | $0{\cdot}148244 \times 10^{-6}$ | 0·630275 | 0·570602 | $-0{\cdot}492604 \times 10^{-2}$ |
| 0·914154 | $-0{\cdot}198682 \times 10^{-8}$ | $0{\cdot}199061 \times 10^{-8}$ | 0·630275 | 0·809570 | $-0{\cdot}145147 \times 10^{-2}$ |
| 1·0 | 0·0 | $-0{\cdot}198033 \times 10^{-7}$ | 0·630275 | 1·0 | 0·0 |

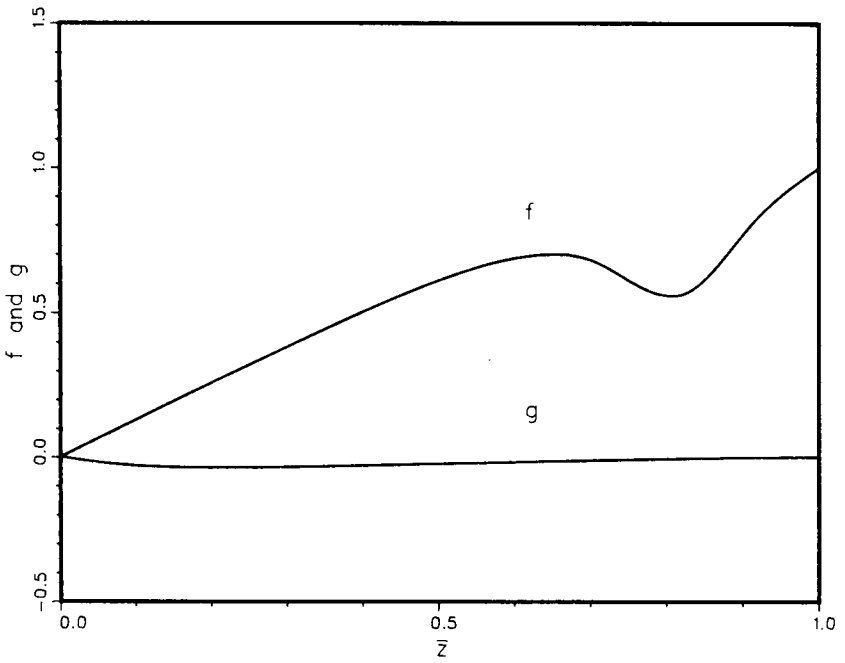


Figure 16. Branch I solution at $s = 0$, $\alpha = 1$, and $C = 1$

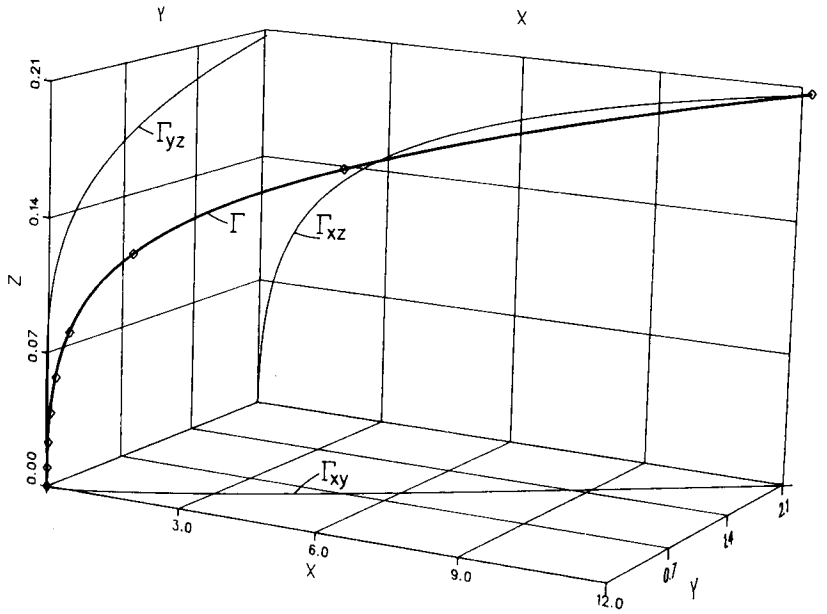


Figure 17. Branch I locus of stagnation points $u = v = 0$; $s = 0$, $\alpha = 1$ and $C = 1$

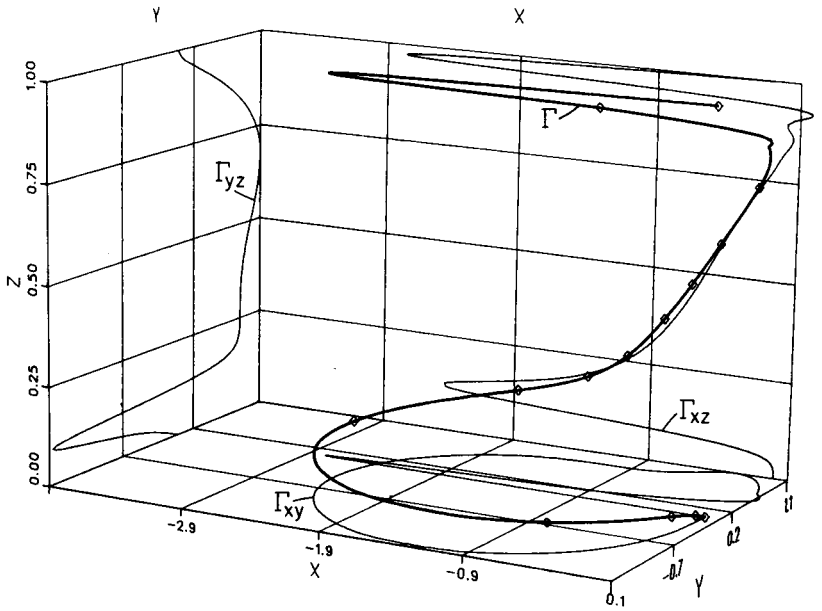


Figure 18. Branch I locus of stagnation points $u = v = 0$; $s = -0{\cdot}257795$, $\alpha = 1$ and $C = 1$

curves of Figures 4–6 at $\alpha = 1$, and with the curves of Figure 15. The second branching occurs at $s = 0{\cdot}0750$. Branches II and III coincide at this value of the parameter $s$; the corresponding von Karman solution is shown in Figure 15. The solutions in this Figure show exceptionally well developed boundary layer structure.

Branch I of the complete asymmetric solution of $s = 0$ and $\alpha = 1$ is given in Table II. We note here that the solution in Table II was obtained on a partition containing 61 internal breakpoints, unequally spaced in accordance with our adaptive mesh generation scheme. Of these we picked out nine breakpoints lying closest to equal spacing and displayed them in Table II. The functions $\{f(\bar{z}), g(\bar{z})\}$ are displayed in Figure 16. The condition $f' \to 0$ as $z \to \infty$ is satisfied by the solution, but is not discernible on the Figure owing to the contracted horizontal scale. The complete velocity field may now be constructed according to equation (2). This velocity field possesses in each $\bar{z} =$ constant plane a point, called here the 'stagnation point', where $u = v = 0$. Figure 17 is an isometric plot of

Table III. Asymmetric flow, branch II: uniform streaming at infinity, $s = 0$, and uniform suction

| $\bar{z}$ | $F$ | $G$ | $-\frac{1}{2}H$ | $f$ | $g$ |
|---|---|---|---|---|---|
| 0·0 | 0·0 | 1·0 | 0·5 | 0·0 | 0·0 |
| 0·104703 | $-0{\cdot}331083 \times 10^{-1}$ | $-0{\cdot}428671$ | $-0{\cdot}761455$ | $-0{\cdot}367073 \times 10^{-1}$ | $-0{\cdot}140755 \times 10^{-1}$ |
| 0·200354 | 0·116450 | $-0{\cdot}96887 \times 10^{-1}$ | $-0{\cdot}111154$ | $-0{\cdot}251314 \times 10^{-1}$ | 0·113596 |
| 0·302749 | $0{\cdot}119453 \times 10^{-1}$ | $-0{\cdot}642388 \times 10^{-2}$ | 0·198644 | 0·141700 | 0·149863 |
| 0·404332 | $0{\cdot}790880 \times 10^{-3}$ | $-0{\cdot}410709 \times 10^{-3}$ | 0·223871 | 0·301567 | 0·130573 |
| 0·499226 | $0{\cdot}604898 \times 10^{-4}$ | $-0{\cdot}314967 \times 10^{-4}$ | 0·225492 | 0·439487 | 0·106747 |
| 0·550247 | $0{\cdot}150308 \times 10^{-4}$ | $-0{\cdot}793594 \times 10^{-5}$ | 0·225592 | 0·504089 | $0{\cdot}936788 \times 10^{-1}$ |
| 0·624436 | $0{\cdot}187047 \times 10^{-5}$ | $-0{\cdot}106384 \times 10^{-5}$ | 0·225622 | 0·563967 | $0{\cdot}747142 \times 10^{-1}$ |
| 0·750941 | $0{\cdot}162671 \times 10^{-7}$ | $0{\cdot}816499 \times 10^{-9}$ | 0·225627 | 0·566923 | $0{\cdot}427976 \times 10^{-1}$ |
| 0·875471 | $0{\cdot}335276 \times 10^{-7}$ | $0{\cdot}414161 \times 10^{-7}$ | 0·225627 | 0·808808 | $0{\cdot}135035 \times 10^{-1}$ |
| 1·0 | $0{\cdot}129143 \times 10^{-7}$ | $0{\cdot}308187 \times 10^{-7}$ | 0·225647 | 1·0 | 0·0 |

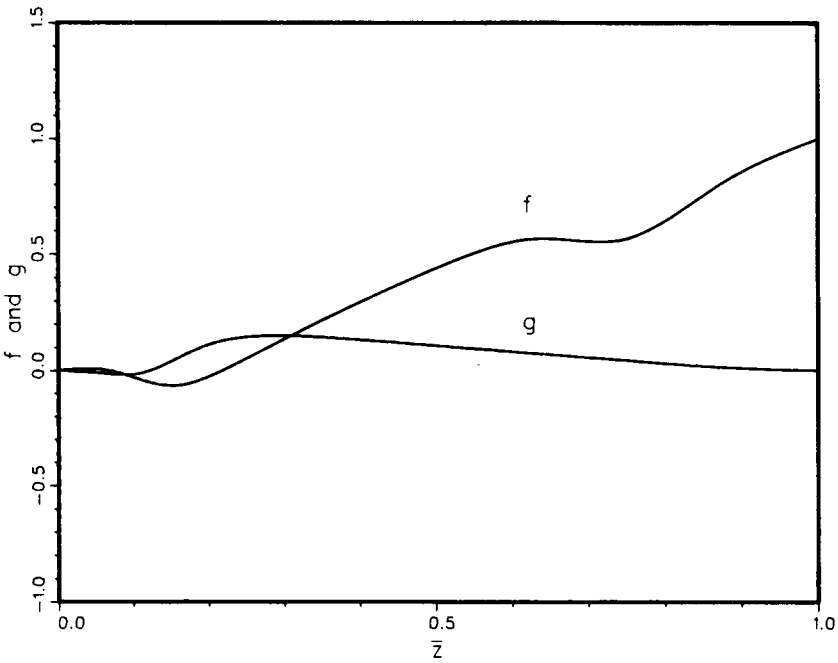


Figure 19. Branch II solution at $s = 0$, $\alpha = 1$ and $C = 1$

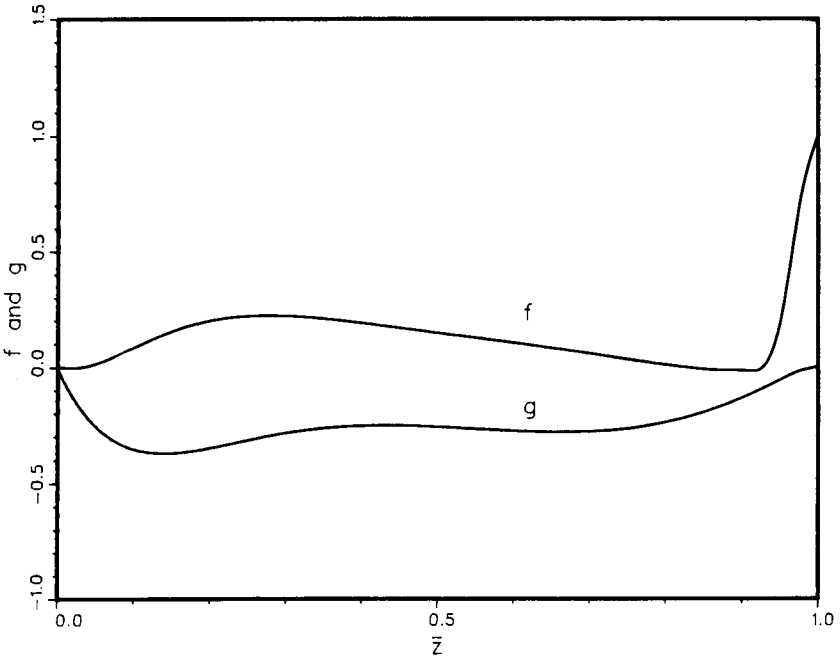


Figure 20. Solution at the first branching point; $s = -0{\cdot}257795$, $\alpha = 1$ and $C = 1$

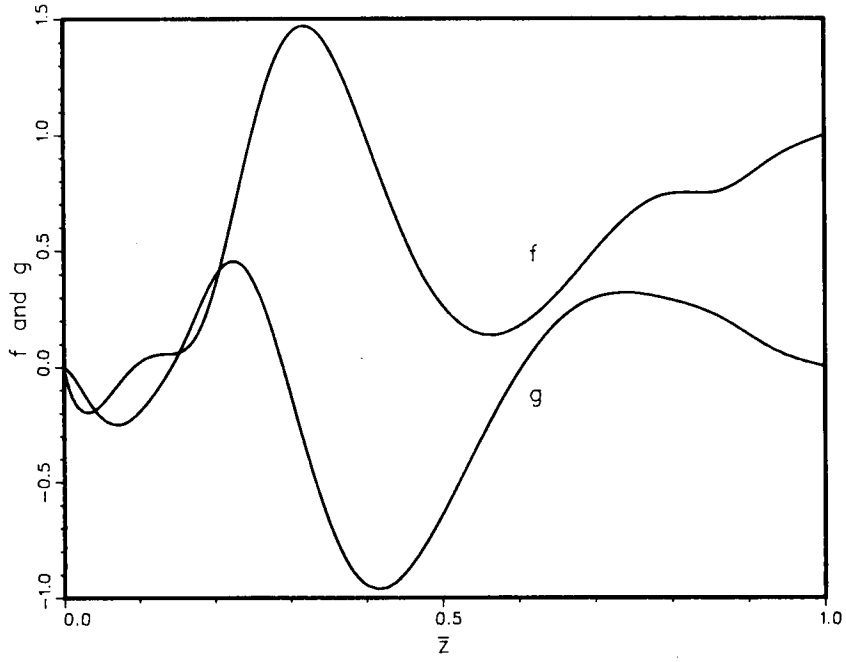


Figure 21. Solution at the second branching point; $s = 0{\cdot}0750$, $\alpha = 1$ and $C = 1$

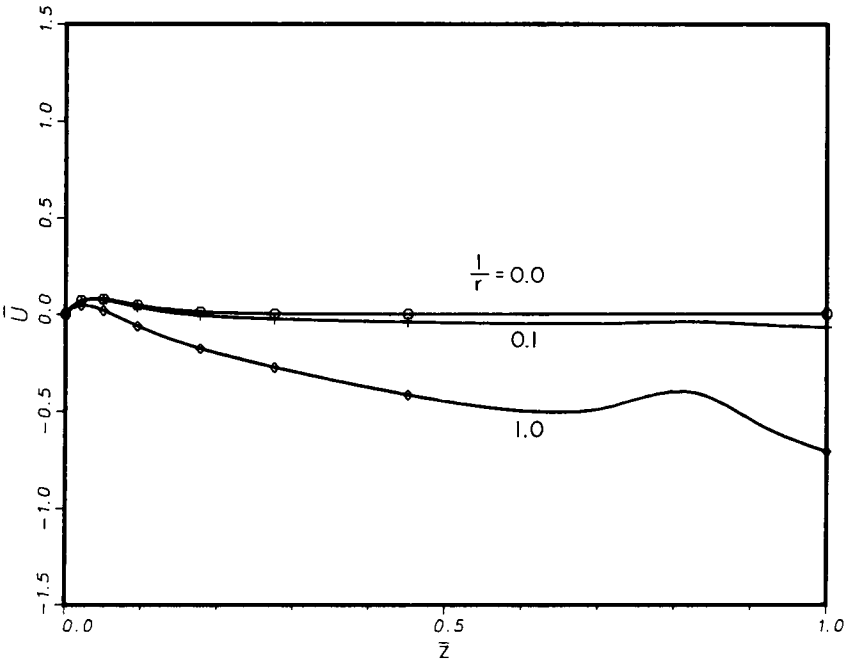


Figure 22. Dimensionless radial velocity $\bar{u} = u/x^1\omega$; $s = 0$, $\alpha = 1$, $C = 1$ and $\theta = \pi/4$

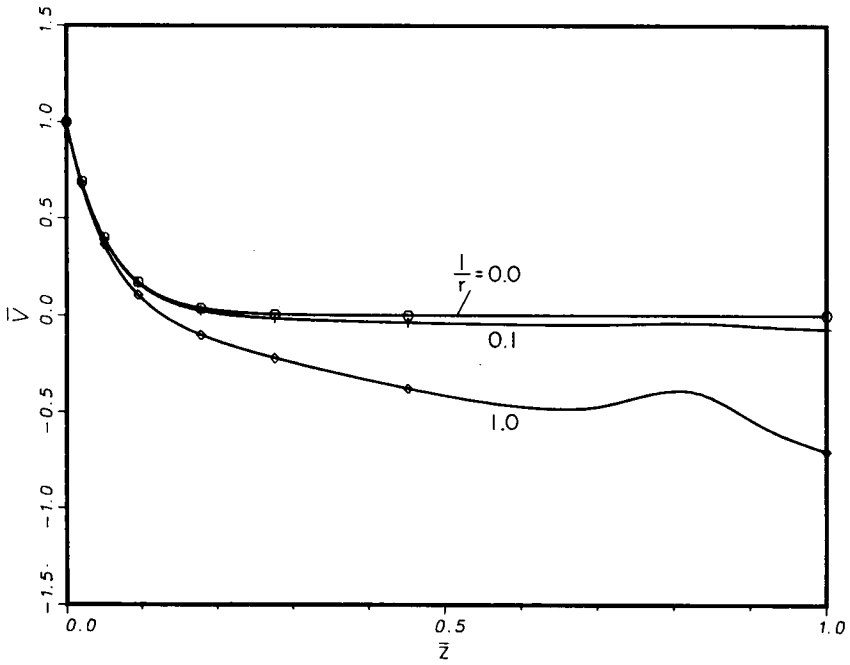


Figure 23. Dimensionless aximuthal velocity $\bar{v} = v/x^1\omega$; $s = 0$, $\alpha = 1$, $C = 1$ and $\theta = \pi/4$

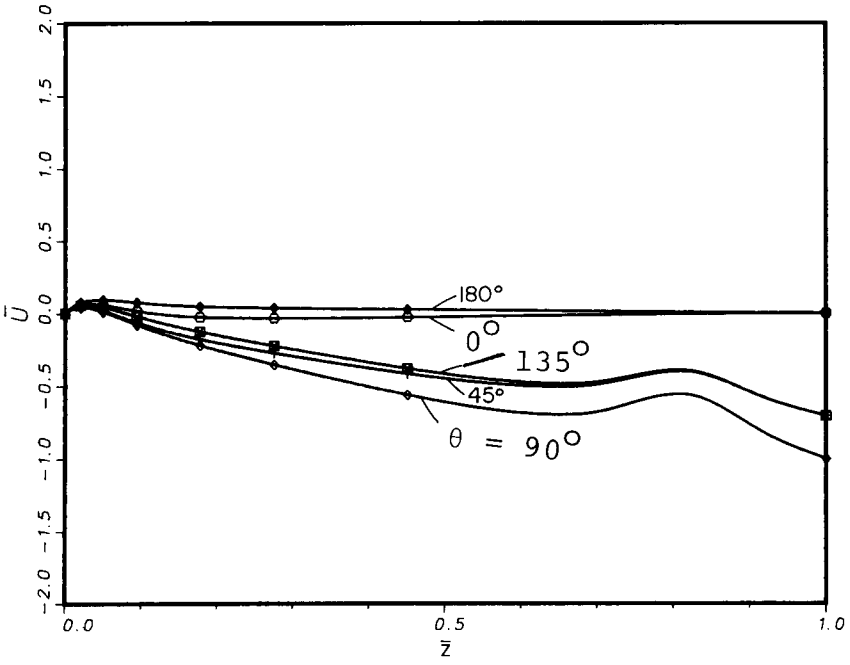


Figure 24. Dimensionless radial velocity $\bar{u} = u/x^1\omega$; $s = 0$, $\alpha = 1$, $C = 1$ and $r = 1$

the locus of $\Gamma$, the stagnation points for the solution in Table II. These are given by

$$\theta = \tan^{-1}\left\{\frac{F(z)f(z) + G(z)q(z)}{G(z)f(z) - F(z)g(z)}\right\} \tag{26a}$$

$$r = \frac{f(z)\sin\theta - q(z)\cos\theta}{F(z)} \tag{26b}$$

The locus of stagnation points for the solution at the first branching point, $s = -0{\cdot}16054$, is shown in Figure 18.

Numerical values at $\alpha = 1$ for branch II of the asymmetric solution are given in Table III. The corresponding curves $\{f(z), g(z)\}$ are shown plotted in Figure 19. There is no discernible boundary layer structure here. Figures 20 and 21 show $f(z)$ and $g(z)$ at the first, $s = -0{\cdot}257795$, and at the second, $s = 0{\cdot}075$, branching points, respectively.

Figure 22 displays the dimensionless radial velocity $\bar{u} = u/x^1\omega$ for $s = 0$, $\alpha = 1$ in various radial positions along the $\theta = \pi/4$ line. Moving inwards from infinity, where the flow is asymptotically the von Karman swirling flow in terms of non-dimensional velocities, the outer layer of the fluid acquires an inward radial velocity. Its azimuthal velocity becomes opposite to the rotation of the disk, as indicated in Figure 23; this Figure shows the dimensionless azimuthal velocity $\bar{v} = v/x^1\omega$ for various positions along the line $\theta = \pi/4$.

Figures 24 and 25 display the flow development at $s = 0$, $\alpha = 1$ encountered by an observer moving along the $r = 1$ circle from $\theta = 0$ in the increasing $\theta$ direction. For small $\theta$ the outer layer seems to possess only axial velocity and an azimuthal velocity that opposes disk rotation (Figure 3). Moving in the direction of $\theta$ increasing, we witness the outerlayer acquire an inward radial velocity and an azimuthal velocity that is in the sense of disk rotation.

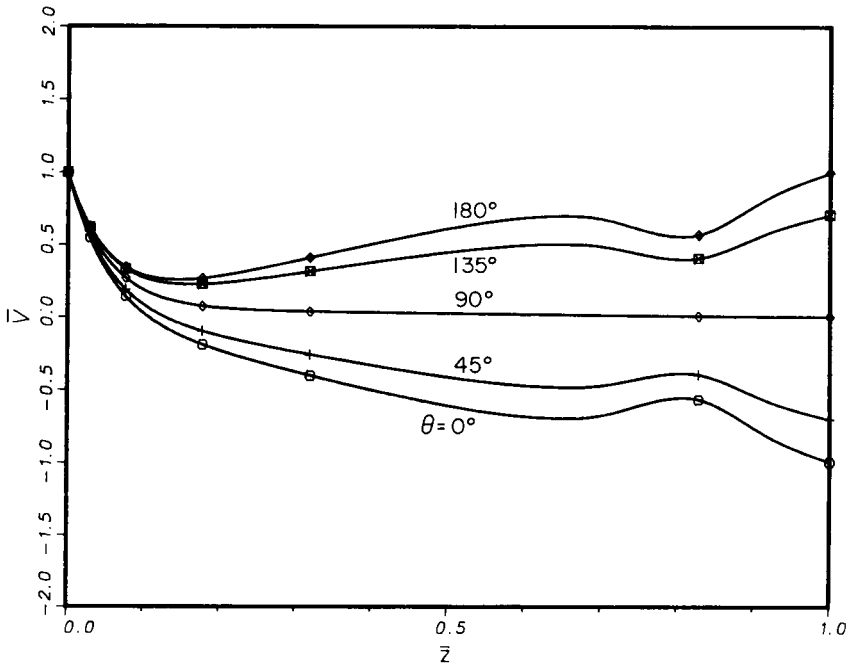


Figure 25. Dimensionless aximuthal velocity $\bar{v} = v/x^1\omega$; $s = 0$, $\alpha = 1$, $C = 1$ and $r = 1$

## CONCLUSIONS

We have, in this paper, calculated a set of previously unknown solutions to the Navier–Stokes equations. A subset of these solutions, obtained with $s = 0$ and $C \neq 0$, corresponds to the flow obtained by placing a rotating disk with uniform suction on the disk into an otherwise uniformly streaming body of fluid.

The solutions obtained here depend on, and are continuous in, an arbitrary parameter $C$, the velocity of streaming at infinity. For zero value of the parameter our asymmetric flow degenerates into the classical von Karman solution. Thus the classical solution is never isolated when considered within the scope of the full Navier–Stokes equations; there are asymmetric solutions in every neighbourhood of the von Karman solution.

The von Karman problem itself exhibits a multiplicity of solutions at zero suction. This also holds true at small, non-zero absolute values of the suction parameter, but for $\alpha < -0{\cdot}82$ and for $\alpha > 1{\cdot}154$ we were unable to locate a second solution.

We also conclude that Galerkin's method with B-spline test functions provides an excellent numerical strategy for non-linear flow problems in the semi-infinite region, when it is coupled with adaptive mesh generation and uses proper asymptotic conditions.

### ACKNOWLEDGEMENT

Extension to asymmetric flows was suggested by Dr. K. R. Rajagopal of the University of Pittsburgh. This is gratefully acknowledged.

### REFERENCES

1. T. von. Karman, 'Uber laminare und turbulente Reibung', *Z. angew. Math. Mech.*, **1,** 233–252 (1921).
2. G. K. Batchelor, 'Note on a class of solutions of the Navier–Stokes equations representing rotationally symmetric flow', *Q. J. Appl. Math.* **4,** 29–41 (1951).
3. J. T. Stuart, 'On the effects of uniform suction on the steady flow due to a rotating disk', *Q. J. Mech. Appl. Math.* **VII,** 446–457 (1954).
4. W. G. Cochran, 'The flow due to a rotating disk', *Proc. Camb. Phil. Soc.*, **30,** 365–375 (1934).
5. M. H. Rogers and G. N. Lance, 'The rotationally symmetric flow of a viscous fluid in the presence of an infinite rotating disk', *J. Fluid Mech.* **7,** 617–631 (1960).
6. P. D. Weidman and L. G. Redekopp, 'On the motion of a rotating fluid in the presence of an infinite rotating disk', *12th Biennial Fluid Dyn. Symp.*, Bialowieza, Poland, 1975.
7. P. J. Zandebergen and D. Dijkstra, 'Non-unique solutions of the Navier–Stokes equations for the Karman swirling flow', *J. Eng. Math.*, **11,** 167–188 (1977).
8. M. Lentini and H. B. Keller, 'The von Karman swirling flows', *SIAM J. Appl. Math.*, **38,** 52–64 (1980).
9. R. Berker, 'A new solution of the Navier–Stokes equation for the motion of a fluid contained between two parallel planes rotating about the same axis', *Arch. Mech. Stosowanej*, **31,** 265–280 (1979).
10. S. V. Parter and K. R. Rajagopal, 'Swirling flow between rotating plates', *Arch. Rat. Mech. Anal.*, **86,** 305–315 (1984).
11. C.-Y. Lai, K. R. Rajagopal and A. Z. Szeri, 'Asymmetric flow between parallel rotating disks', *J. Fluid Mech.*, **146,** 203–225 (1984).
12. C.-Y. Lai, K. R. Rajagopal and A. Z. Szeri, 'Asymmetric flow above a rotating disk', *J. Fluid Mech.*, **157,** 471–492 (1985).
13. C. de Boor, *A Practical Guide to Splines*, Springer, 1978.
14. R. D. Russel and J. Christiansen, 'Adaptive mesh selection strategies for solving boundary value problems', *SIAM J. Numer. Anal.*, **15,** 59–80 (1978).